Spring 5-21-2020

Detection of Mild Cognitive Impairment using Diffusion Compartment Imaging

Matthew Jones

Detection of Mild Cognitive Impairment using Diffusion Compartment Imaging

A project

Presented to

The Faculty of the Department of Computer Science

San José State University

In Partial Fulfilment

Of the Requirements for the

Degree Master of Science

Committee Members:

Dr. Leonard Wesley

Dr. Allyson Rosen

Dr. Yulia Newton

By

Matthew Jones

May 2020

ABSTRACT

The result of applying the Neurite Orientation Density and Dispersion Index (NODDI) algorithm to improve the prediction accuracy for patients diagnosed with MCI is reported. Calculations were carried out using a collection of 68 patients (34 control and 34 with MCI) gathered from the Alzheimer's Disease Neuroimaging Initiative database (ADNI). Patient data includes the use of high-resolution Magnetic Resonance Images as with as Diffusion Tensor Imaging. A Linear Regression accuracy of 83% was observed using the added NODDI summary statistic: Orientation Dispersion Index (ODI). A statistically significant difference in groups was found between control patients and patients with MCI with a power 0.96. In order to confirm performance, comparison of accuracy of prediction without the use and with the use of the ODI values is also presented. The impact of this increase in accuracy on the early detection of MCI is also presented. Results show a 4.68% increase in prediction accuracy through the inclusion of the ODI values. Future work includes the use of tractography to better locate the specific area of interest. Increasing the cohort would also add validity to the results in this paper. Expanding the number of tracts utilized in this study would also validate the use of the NODDI algorithm to detect neurological deterioration in tracts associated with memory. The inclusion of more complex prediction models would also add possible increases in performance in modeling patients with MCI.

Key Words: Mild Cognitive Impairment, Computer Vision, Diffusion Compartmental Imaging, NODDI, Alzheimer's Disease

Table of Contents

List of Tables

List of Figures

INTRODUCTION

Mild Cognitive Impairment is defined as cognitive dysfunction without functional disability and this entity is believed to be an early stage of degenerative brain disorder that progresses to dementia. Dementia is a syndrome characterized by cognitive decline in one or more areas of cognition including memory and that cognitive decline must be characterized as being enough to interfere functioning, activities necessary to conduct the day to day life of the patient (Jalbert, Daiello, & Lapane, 2008; Lyketsos et al., 2006). Dementia can result from a spectrum of brain diseases that include Alzheimer's Disease, vascular dementia, Parkinson's dementia, all of which have cognitive and functional disability.

Alzheimer's Disease (AD) is a fatal disease defined as the global deterioration of memory and other cognitive domain (Jalbert et al., 2008). The prevalence of Alzheimer's tends to increase with age with an occurrence of 1 in 1,000 people between the age of 60-64 and 25 per 1,000 for those above the age of 85 developing the disease (Jalbert et al., 2008; van Duijn, 1996). 1 to 2 percent of healthy adults progress to developing Alzheimer's Disease each year (Bischkopf, Busse, & Angermeyer, 2002). For patients with Mild Cognitive Impairment the chance of conversion is much higher at 10 to 15 percent per year (Bischkopf et al., 2002; Knopman & Petersen, 2014).

Mild Cognitive Impairment (MCI), as opposed to Alzheimer's, is more subtle. MCI is defined as an in-between state where the patient has cognitive limitations but functionality is generally intact but there may be subtle difficulties in functioning. This distinction does not lie under the definition of dementia, but still remains to inhibit the patient's day to day life (Petersen, Doody, et al., 2001; Petersen, Stevens, et al., 2001; Rivas-Vazquez, Mendez, Rey, & Carrazana, 2004). The general criteria

for the diagnosis of MCI can be broken down into 5 points taken from Petersen et al. (1999):

- Patient reports complaints of memory issues, which would be corroborated by a trusted third-party.
- Difference from the age norm of 1.5 standard deviations on a memory impairment test.
- No other issues in cognitive functioning.
- Does not meet the criteria for Dementia.
- Ability to perform day-to-day functioning including driving a car.

Mild Cognitive Impairment and Alzheimer's Disease currently affect 16 million and 5.1 million people world-wide respectively. The number patients diagnosed with Alzheimer's disease is estimated to rise to 13.2 million by 2020 and according to Brookmeyer, Johnson, Ziegler-Graham, and Arrighi (2007) by 2050 1 in 85 people will be living with Alzheimer's disease. This increase can be reduced through the practice of early detection and therapies. If early intervention can cause a 1 year decrease in the onset of the disease an estimated 9.2 million fewer cases will occur by the year 2050 (Brookmeyer et al., 2007).

Current best practices for diagnosing MCI in a clinical setting involves conducting a thorough assessment of a subject's overall physical and cognitive health (Albert et al., 2011). This includes a number of examinations primarily focused on excluding alternative diagnoses through a review of a patient's medical history, diagnostic questionnaires, and cognitive evaluation (Neugroschl & Wang, 2011). The most common early difficulty is memory dysfunction. One of the most challenging and sensitive measures is list learning and the most commonly used measure is the RAVLT (Rabin et al., 2009). Ultimately as AD progresses other cognitive domains are involved and a screening measure such as the Montreal Cognitive Assessment

(MoCA). Although short, it is used to describe the severity of dementia and surveys multiple cognitive domains. These measures include items sensitive for memory and hence can be used to detect MCI but is relatively less sensitive to memory dysfunction than RAVLT. Whereas there is a general consistency in the types of information leading to a diagnosis, not all people with symptoms of MCI progress to AD and hence additional imaging and other biomarker data are being incorporated in research diagnosis with the goal of clinical use.

One approach to improving the early detection of preclinical AD is to focus detecting the earliest degenerative changes in the medial temporal lobe (MTL). This region is responsible for memory. Previous studies have demonstrated correlations between memory ability and MRI volume (Moradi, Hallikainen, Hanninen, Tohka, & Alzheimer's Disease Neuroimaging, 2017). Because AD degeneration is progressive, one would expect that there would be longitudinal change in the structural differences between MCI and healthy older adults.

Combining minimally invasive neuroimage-based measures of localized structural changes in the brain over time with other cognitive measures appears promising as the basis of a more effective MCI diagnostic approach than is currently available.

This lack of combination in the field provides us with a technical gap in the current literature that we wish to address in this report. Whereas there have been multiple studies of MTL atrophy, white matter changes in the MTL have not been extensively studied (Goldman et al., 2017; Wen et al., 2019).

Neuroimage-based analysis includes the use of systems that that model the intricacies of the brain’s internal structure and architecture. From these models, summary statistics are generated. These statistics are then used to further analyze group differences. One such analysis presented in this report is Neurite Orientation Density and Dispersion Index (NODDI). NODDI produces a summary statistic that

characterizes the orientation dispersion of axon bundles. Analysis from NODDI utilizes shape distributions that closely resembles the shape and make up different types of tissues found in the brain. The analysis and application of this algorithm is presented in this report.

BACKGROUND

The brain changes of AD appear about a decade before the symptoms appear. MCI is a transition stage when there is cognitive dysfunction detectable by neuropsychological testing but before the progression to the disabling functional incapacity of Alzheimer's dementia (Bateman et al., 2012; Golomb, Kluger, & Ferris, 2004; Roberts et al., 2014). During this period the brains of people with neuropathology is deteriorating at a rate greater than those with healthy brains. Diagnosing at or before the complete deterioration of the brain is important to the longevity of the patient and the impact on the medical system (Brookmeyer et al., 2007).

Clinical Diagnosis

The current clinical diagnostic criteria for Mild Cognitive Impairment primarily focuses on whether the patient experiences cognitive declines but functional decline in everyday life is minimal (Albert et al., 2011). Examples of difficulty functioning include writing checks, shopping alone, playing a game, making a cup of coffee, etc. and whether these tasks have been inhibited by any sort of memory issue (Pfeffer, Kurosaki, Harrah, Chance, & Filos, 1982; Teng et al., 2010). Neuropsychological tests are critical for diagnosis. Whereas memory is typically the earliest symptom of AD, other cognitive domains can be diminished including language, attention and mental control, and visuospatial functioning.

A variety of paper and pencil neuropsychological tests are typically used. One such test which this project utilizes is Rey Auditory Verbal Learning Test, or RAVLT

(Schmidt, 1996). RAVLT, originally created by Andre Rey, a Swiss psychologist, was developed to assess verbal memory in patients 16 and older. RAVTL has shown through multiple studies to play a significant role in the early detection of early onset Alzheimer's (Estevez-Gonzalez, Kulisevsky, Boltes, Otermin, & Garcia-Sanchez, 2003; Moradi et al., 2017). Brain volume has also shown to be a predictor of a patients RAVLT score with a has been shown to be a predictor for brain volume as detailed by Moradi et al. (2017). For more information regarding the intricacies of RAVLT and how it is run please refer to Appendix A.

The second test considered in this project is MoCA or Montreal Cognitive Assessment. MoCA, created in 1996 by Ziad Nasreddine, a Canadian neurologist, was specially designed for the early detection of Alzheimer's (Neugroschl & Wang, 2011) and has shown to be a highly sensitive screening measure that briefly surveys multiple cognitive domains including memory (Nasreddine et al., 2005). Whereas memory decline is the most common domain affected early in AD, in some subtypes of AD other domains are affected hence a global screening measure is an important additional measure. Because AD patients often lack insight into their functional difficulties and have deficits in several domains, a score on MoCA that is too low is also a warning sign that the patient has progressed beyond the stage of MCI to AD. For more information regarding the cut offs and ranges of different stages, please refer to Appendix B.

Diagnosis Using Neuroimaging

Although these tests have shown to be decent predictors of future progression to AD, they exhibit high rate of false positives, which warrants exploring other options for diagnostic tests. Having convergent data from neuroimaging can increase accuracy of the diagnosis. Historically clinicians relied on postmortem analysis to identify the AD brain pathology; however, presently PET identifies

both tau and amyloid pathology. Another such technology is Magnetic Resonance Images (MRI) which has the advantage of not requiring injection of radioactive tracers like PET. MRI uses powerful magnets to change the direction of spin of hydrogen atoms in the patient's bodies. Some of the hydrogen atoms will align to the new magnetic direction imposed. Of these newly facing directions exist some hydrogen atoms that face in opposing directions to their local space's magnetic direction. This change in direction is then interrupted using powerful radio signals which then causes these standouts to align back to the herd's original direction. This sudden change releases energy which is then read by the detector facing the patient. The energy is then converted to digital images. These images provide a key point in the examination of the flow of water in the brain of the patient. Depending on the way the MRI is created, different brain tissues have different values, displayed to clinician as brightness or intensities. This information is clinically important and can be compared to learn about the locations of the brain and integrity of its functioning. With sophisticated analytic techniques that compare the locations of the brain both within and across, information researchers can derive additional insights.

This project relies on two types of images: structural T1 weighted images, and a Diffusion Weighted Image (DWI). On a structural, T1 image, the surface of the brain (cortex, grey matter) is grey and underneath the cortex the brain appears white (denoted white matter). This difference in intensity is critical information about the role of those brain regions. Information regarding grey and white matter can be found in Appendix C.

Diffusion Weighted Images are a different kind of image that instead is sensitive to white matter tracts. Typically, white matter is organized as groups of axons or fibers tracts and to the extent those fibers are healthy/intact and/or the brain region

that DWI will vary in intensity. The technique depends on the fact that DWI is sensitive to the degree to which water diffuses along these axons or fiber tracts. Variation in diffusivity can be thought of conceptually as water moving along a straw. Movement on the outside of the straw is unrestricted this is coined as “Free Diffusion”. Much like the walls of a straw, water does not diffuse from the outside to the inside of the straw. DWI thus generates an image that varies in Free Diffusion and Diffusion Restriction. Included with this image is two metadata points that characterize the gradient’s strength and timing at the moment of acquisition; this is included as a “b-value”. The gradient directions at said time is also included as a “b-vector”. An example of such an image can be seen in Figure 1. The image contains a processed Diffusion Weighted Image. Areas of diffusion restriction are indicated through bright white intensities, whereas areas with less are darker in intensity.

Figure 1: Diffusion Weighted Image Example

Free diffusion is shown as bright white spots on the image and indicates the ability for water in that sector to freely diffuses in any direction. Conversely, diffusion restriction indicates limited diffusion in that area and as a result the intensity is lower.

The field studying AD has focused on measuring grey matter volume, typically in the hippocampus and related medial temporal lobe (MTL) structures and less so on white matter fiber tract degeneration, hence DWI has been less frequently applied in the prediction of MCI/Alzheimer's (Miller et al., 2015).

Whereas DWI represents brain locations in terms of their diffusivity, to represent fiber tracts involves complex analyses. Diffusion Tensor Imaging (DTI) is a method of analysis that uses water diffusion to map, detect, and detail tracts of

axons, the long, glia encased fibers that connect the bodies of neurons (grey matter).

Diffusion Tensor Imaging

DTI analysis was originally proposed by Peter Basser (Basser, Mattiello, & LeBihan, 1994a, 1994b) and relies on the concept of a diffusion tensor. An image analyzed by Diffusion Tensor Imaging contains a multitude of points called voxels (or volumes in 3d space). Each of these voxels in the brain model either one of three types of tissues in the brain: white matter, grey matter, and cerebral spinal fluid. DTI analysis of these voxels provide a general model of inherent characteristics of the tissue analyzed. In-order to produce this general model a series of processing steps needs to occur and, depending on the source of data, can be prone to errors as a result much preprocessing needs to take place (Soares, Marques, Alves, & Sousa, 2013). These steps are detailed later in the Methods section. More information regarding the background of diffusion tensor imaging is included in Appendix D.

Diffusion Tensor Imaging's main parameters: Mean Diffusivity (MD) and Fractional Anisotropy (FA) have seen use in predicting atrophy among patients along the spectrum of degeneration. Selnes et al. (2013) utilizes DTI in a way to further predict, using regression, atrophy among patients with subjective and mild cognitive impairment. Selnes et al. (2013) found, through a targeted study in the medial temporal lobe, that MD and FA were significantly associated with atrophy ($p < 0.05$). For the regression analysis, MD was found to be able to predict atrophy whereas FA was not.

In Bozzali et al. (2002) FA was found to be a statistically significant difference between the controls and AD group ($p < 0.01$). The areas of interest that produced

the lowest p value includes: the corpus callosum, frontal, temporal, and parietal lobe.

Although these statistics have seen wide use, DTI is not without its pitfalls. There is a general recognition that in brain locations where postmortem dissection identifies that densely packed fiber tracts cross or axonal bundles join, the results of analysis conducted in these areas are ambiguous. Because DTI works on a voxel per voxel basis these overlaps hinder the analysis of Fractional Anisotropy (Tournier, Mori, & Leemans, 2011).

Technical Gaps

When using DTI models, a lot of key information is lost through its ambiguity. In-order to address this difference in tissue modeling a multi model method must be used, one for each type of tissue. This multi model method, otherwise known as Diffusion Compartmental Imaging, provides a deeper insight into those regions that might be hindered through a flat analysis of the entirety of the brain. To close this technical gap, we utilize this method in conjunction with available cognitive tests including RAVLT and MoCA to provide a robust implementation. For more information and background regarding Diffusion Compartment Imaging please refer to Appendix E.

APPROACH

Data

The Alzheimer's Disease Neuroimaging Initiative (ADNI) database founded by Principle Investigator Michael W. Weiner, MD in 2003 was the primary supplier of Data utilized in this project. The supplied data contains that of a multitude of mediums including Magnetic Resonance Imaging (MRI), clinical assessments, neuropsychological assessments, Positron Emission Tomography (PET), and biological markers. The intent of the project is to test the viability of these mediums

in the pursuit of measuring the progression of Mild Cognitive Impairment (MCI) and early Alzheimer's disease (AD).

The database acts as a hub for a variety of studies related to Alzheimer's and contains several patients who are on the spectrum between normal cognition (NC) and dementia.

The database is primarily broken up into 4 participant stages 1, GO, 2, and 3 with 3 being the focus of attention for this project. ADNI3 is the latest in the line of studies starting from 2016 onward and concluding in 2022. This cohort includes several patients including 133 elderly controls, 151 patients with MCI, and 87 patients with Alzheimer's disease.

Included in the ADNI study are a wide variety of imaging types. Of those types this project focuses on two types: Structural and Diffusion Imaging.

Structural Imaging

The primary purpose of Structure Imaging (T1) is to visualize the entirety of the brain and produce clear delineation of tissue types. This includes highly detailed and highly contrasted images that convey the internal structures of the brain. The primary way of acquiring this structural imaging is with magnetic resonance imaging (MRI). This type of imaging includes T1 and T2-weighted images. Our study primarily focused on T1 images. This type of imaging removes variations in the resulting image of the brain and provides a high amount of resolution for clearer analysis (M Symms et. al.).

The use of this type of image in our methods provides for a greater ability to segment portions of the brain known as white matter, grey matter, and cerebrospinal fluid (CSF). Through this we can clearly see the differentiation between the three and as such generate masks related to these areas. As detailed in our analysis methods, this

is a pivotal implementation that gives us the ability to extract out a specific portion of the brain for use in the later analysis. Specific to the T1 image utilized, we focused on using ones generated through the 3D Magnetization-prepared rapid gradient-echo (MPRAGE) sequence. MPRAGE has shown to be well-established across studies over a period as well as studies that occur at different sites or labs (Falkovskiy et. Al). MRPAGE also provides high contrast which allows for a clearer differentiation between tissues (Falkovskiy et. Al).

Diffusion Imaging is the prime focus for this project and provides the underlying data that is operated on in order to produce our summary statistic. Diffusion Imaging is a technique used to measure the diffusion of water through the brain. This diffusion details the motion of water molecules present in the brain. Through this information we can identify the direction of this flow using a variety of techniques.

Cohort

The cohort analyzed consists of 34 control subjects and 34 patients diagnosed with mild cognitive impairment. Each diagnosis of the patients was taken directly from the ADNI3 dataset and were the result of a consensus diagnosis of experts.

Of this cohort, the distribution of age acted as a nuisance parameter for the analysis of whose distribution is referenced in Figure 1. The distribution of controls indicating a flatter curve than the mci patients.

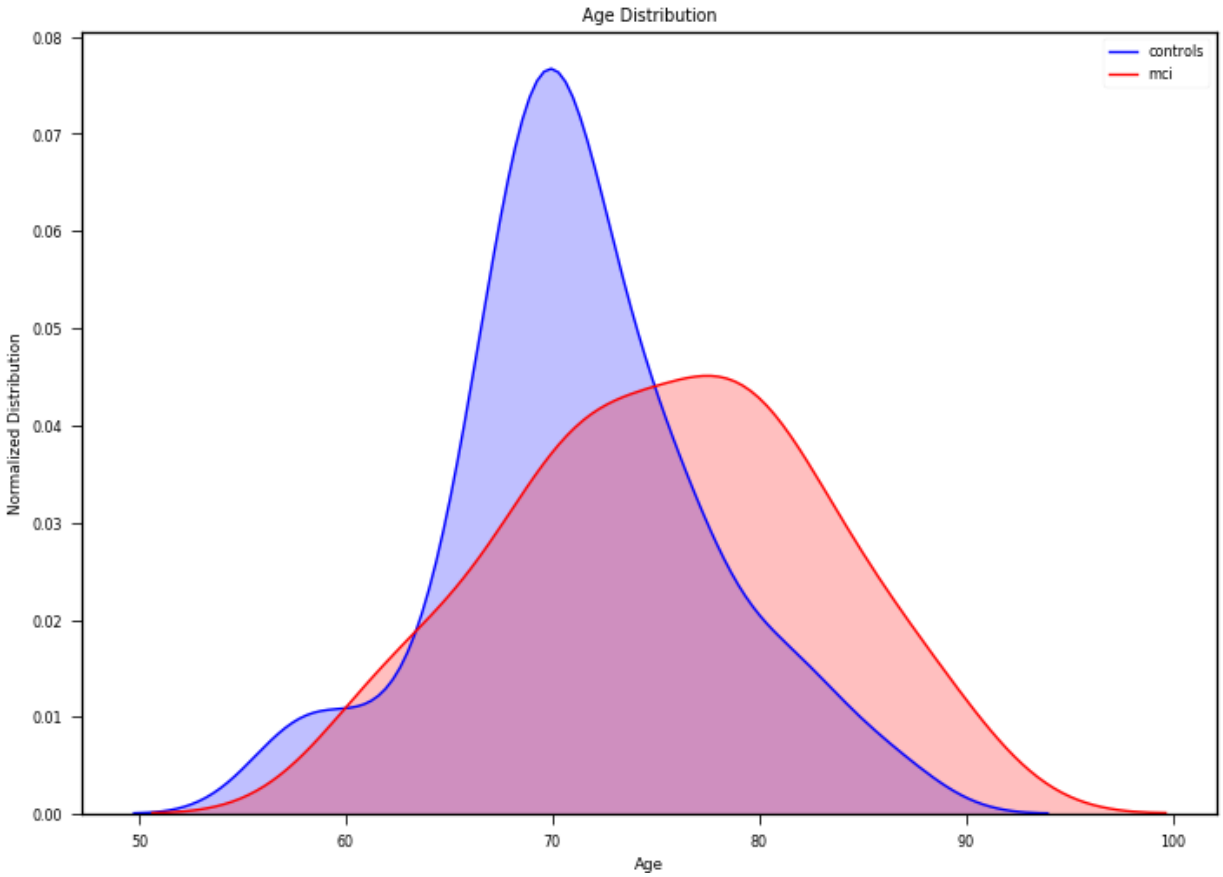

Figure 2: Age Distribution of ADNI3 Patients

The cohort also consists of a minimum of two time-series data points. Two runs over the period of a year: one at a baseline and one at a one year follow up were conducted.

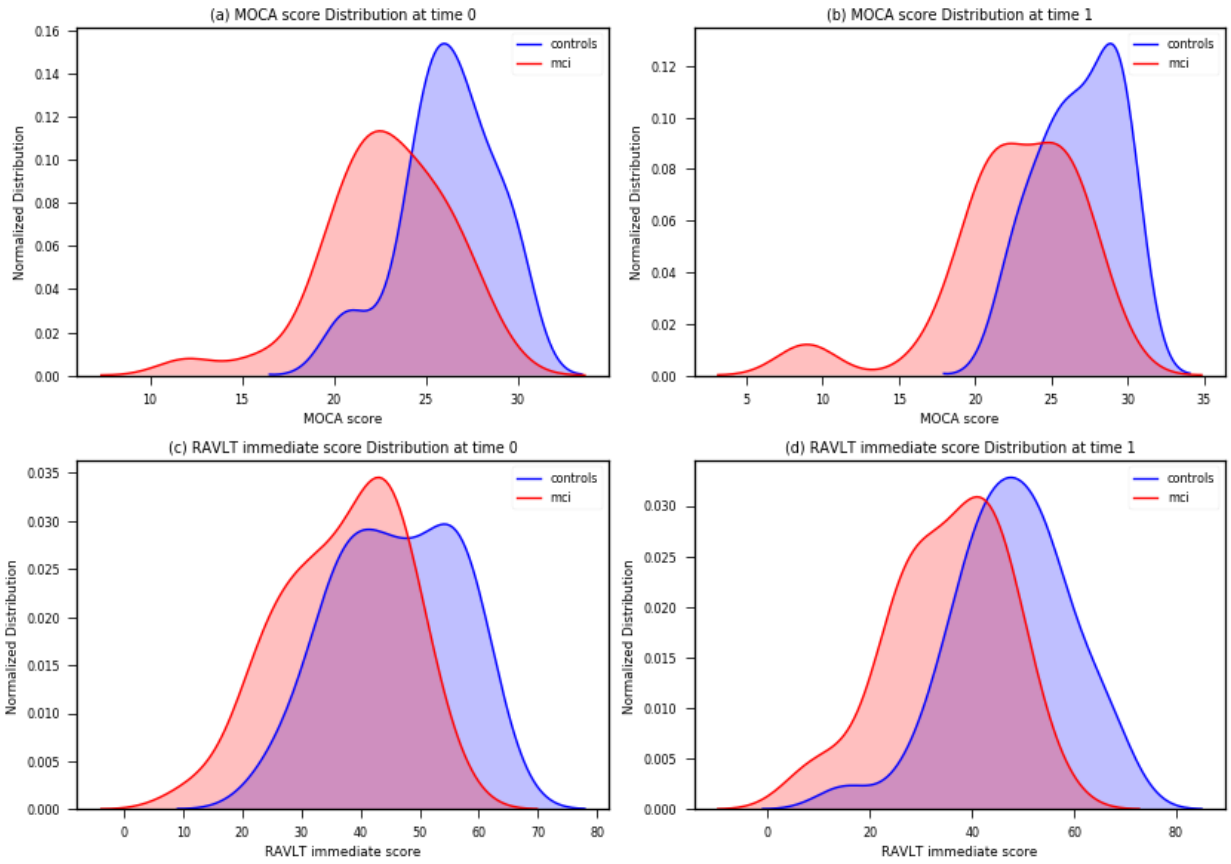

Figure 3: (a) MOCA score Distribution at time 0 (b) MOCA score Distribution at time 1 (c) RAVLT immediate score Distribution at time 0 (d) RAVLT immediate score Distribution at time 1

The analysis utilized in this study is the previously described Diffusion Compartmental Imaging (DCI). The specific algorithm utilized is Neurite Orientation Dispersion and Density Imaging (NODDI). This method was used in conjunction with a large number of data pre-processing and manipulation steps, which utilize the FMRIB Software Library (FSL). FSL includes several packages that help in the processing and analysis of MRI data. Among those packages included, this project specifically utilized seven: fslreorient2std, BET, eddy_correct, flirt, fast, fslsplit, and fslmaths.

The pipeline for the analysis of the patient data is detailed below.

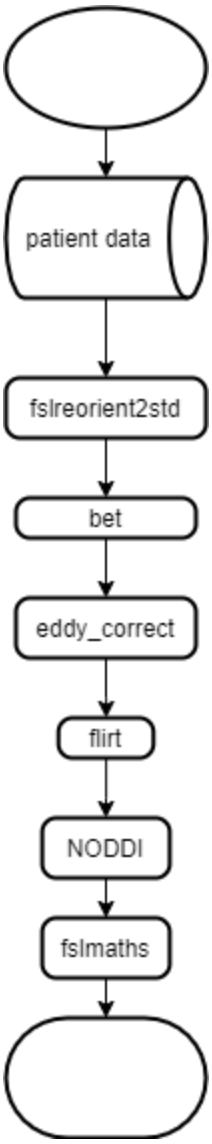

Figure 4: General Analysis Pipeline

The entirety of the pipeline is broken down into three sections. The first step includes the preprocessing and formatting of the patient data. This includes the following FSL packages: fslreorient2std, bet, eddy_correct, and flirt. The second step, being the run of NODDI on the pre-processed patient's data. The last being the post-processing step that includes the use of a variety of masking tooks such as: fslmaths and optionally (if not done already) fslsplit.

Pre-Processing

The goal of this preprocessing step is to fulfill the preconditions for the analysis. The first condition is that the patient's data be registered correctly to MNI space. This space refers to a known orientation and coordinate system generated from an average of 152 images of human brains. This registration allows for the targeted analysis of specific portions of the brain using known coordinates. The template used in this stage is the MNI 152 average template (Brett, Johnsrude, & Owen, 2002) included in the default FSL data.

The first step of this four-step process is to utilize the fslreorient2std tool. This tool acts as a simple reorientation script to the MNI 152 template. It reorients it in such a way that the brain is in the same orientation in the left and the right space and is directly on top of the MNI template. This allows for a registration process that is least error prone.

The second step is to utilize the BET tool also included in FSL. BET is a simple brain extraction tool. From patients MRI and DTI, it produces an image that only includes the actual brain itself. This is used to exclude parts of the image included in the raw base image of the patient's brain. These parts might include the outer portion of the skull, the eyes, and any other part outside the scope of interest. This result is the stripped image and is then fed into the next stage: eddy_correct.

Eddy_correct or simply eddy, is a tool for use in the correction of eddy current-induced distortions and subject movements for diffusion imaging (Andersson & Sotiropoulos, 2016). This tool allows for the correction of possible imperfect acquisitions of patient's brains during the process of collecting the diffusion of water molecules in the brain (DTI). It "corrects for distortions by registering the individual models to a model free prediction of what each volume should look like" (Andersson & Sotiropoulos, 2016). These corrections allow for the use of images that would

otherwise be error prone due to issues at the collection stage. After this stage is complete the results are then fed to the registration stage.

The tool used for this registration stage is the flirt tool supplied by FSL (Jenkinson & Smith, 2001) (Jenkinson, Bannister, Brady, & Smith, 2002). Flirt or FMRIB's Linear Image Registration Tool is a tool for automatic linear brain image registration. Image registration is the process with which one image is transformed from its coordinate space to another images coordinate space. This is the key point of this section. The registration of the DTI and MRI image puts them both into "MNI space". MNI space is a well-known probabilistic atlas developed at the Montreal Neurological Institute. Individual brains are reshaped or warped to match the atlas so that overlaying them increases the likelihood that functional areas align. With this transformation images can be analyzed together in voxel-based space rather than by manual tracing base on the shape of different brain regions.

The atlas has been used to derive a vast number of masks or clusters of voxels that align with prior defined brain regions. These masks can be multiplied by whole brain images to select these regions. For example, with a binary mask in which the target brain voxels have the value of 1 and non-target brain regions have the value of 0, a multiplication of these images selects the target brain region eliminating all other regions. This masking is one of the reasons for this pre-processing step as detailed in the post-processing step. Having both images also registered in this space allows for a consistent analysis across cohorts as all the images of the brains in this cohort have been transformed into a common space. Once transformed the cohort's brains can then be reliably compared knowing that the sample space each have been pulled from is normalized.

Analysis

The second section of the pipeline includes the running of the NODDI algorithm. This stage can be broken down into several sub-steps described below:

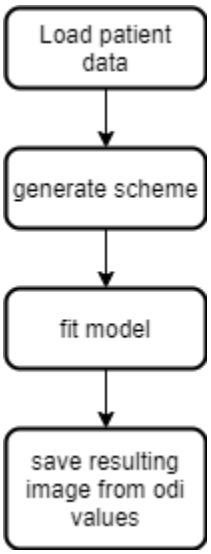

Figure 5: NODDI process

The first step being the loading of the patient data into memory. This includes the NIFTI1 formatted Diffusion Tensor Image resulting from the previous stage, the b-values, and the b-vectors. The NIFTI1 image format (otherwise shown as nii) is a format that provides a wrapper around the image which includes several features. Among these features includes the affine related to that image as well as any labels or meta data. This type of data was read using the nibabel python package. During this loading process the patient's b-vectors and b-values are read into a gradient table through the use of the DIPY package (Garyfallidis et al., 2014). This gradient table takes in the locations of the bval and bvec files, loads, and formats them accordingly. In this loading there are several quality checks to make sure each are valid.

Once the nii, bval, and bvec files are loaded the main package utilized then translates that gradient table into a scheme for use in the calculation of our model. The scheme is utilized from the dmipy package and is the main encapsulation of the data needed to simulate and train the model (Fick, Wassermann, & Deriche, 2019). The model

utilized in this training step is comprised of three shells: a plane ball model, and a Watson dispersed bundle of a stick and zeppelin model. This model comprises the Neurite Orientation Dispersion and Density Imaging (NODDI) (Zhang, Schneider, Wheeler-Kingshott, & Alexander, 2012). The NODDI model is then fit over the entirety of the patient's brain. The dmipy package includes two main packages for performance enhancing: pathos (Michael M. McKerns, 2012; Michael McKerns, 2010-) and numba.

Once the model is fitted the resulting parameters are then extracted. The primary summary statistic this project focuses on is the ODI values or orientation dispersion index. The ODI values are included in a range from 0.0 – 1.0 and are calculated per voxel. Through this voxel calculation an image of the brain from these values is generated and is then saved using the original diffusion tensor image affine. This resulting image has the same properties as the original registered image, allowing us to proceed to the post-processing stage.

Post-Processing

The proceeding stage after the analysis of the pre-processed images includes several masking steps and calculations based on the resulting ODI image shown below:

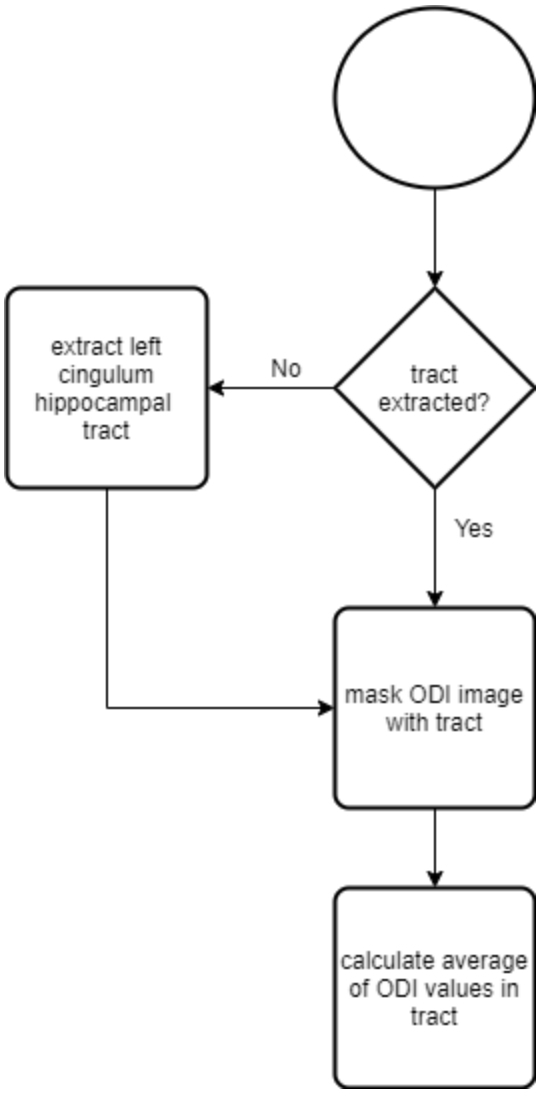

Figure 6: Flow Chart of Post-Processing Steps

The post processing step includes the extraction of the specific tract being studied through the use of a mask. For this study we used the cingulum hippocampal tract. This tract was pulled from an atlas included in FSL from the Laboratory of Brain Anatomical MRI in Johns Hopkins Medical Institute (Hua et al., 2008; Nagae-Poetscher, 2005; Wakana et al., 2007). This atlas includes a multitude of masks built in MNI space. Since the results of our fitted model were calculated in MNI space this result can then be utilized to look at specific portions of the brain. Using

fslmaths we utilize the atlas related to the cingulum hippocampal region to extract the region of interest.

Once extracted the resulting masked image is then loaded using nibabel and the results are then calculated using the masked average value of the region. This resulting average is the metric utilized in our statistical study of these trails.

Modeling

Once the ODI values are extracted the resulting average of the region specified is then added to an excel file that details the patient's metadata. This metadata includes the patient's RAVLT and MoCA score. Two Linear Regression Models are then trained for the use in predicting subjects with MCI.

The first model includes the mentioned RAVLT and MoCA scores along side the ODI values. The values are taken at both intervals and differenced between time 0 and time 1 (baseline and a 1-year follow-up) then a product is taken between the combination of the three differenced categories. The second model then produces the same combination but with the exclusion of the ODI values. The second model then serves as a benchmark to test the degree with which the inclusion of ODI values can help predict MCI subjects.

Context

The analysis of the 73 participants (comprising patients and controls) was ran on the San Jose State University Spartan01 High Performance Computer. The Spartan01 contains 72 compute nodes, 2 high memory nodes, and 4 GPU nodes for a combined number of 2152 of compute cores and 23040 GPU cores. The Spartan01 runs slurm workload manager. Through Slurm the patients were able to be ran concurrently across 5-6 nodes for a total of ~200 individual runs. Each run contained ~500 megabytes of data.

In-order to run the patient's data on the High-Performance Computer (HPC) the data first needs to be transferred. The procedure for transferring the data first starts with the downloading of the individual patient files from the ADNI server. The individual patients contain an average of two years of data. Each year contains 2 data points: The T1 MRI and the Axial DTI image which are both DICOM formatted image files.

Once downloaded the files require a formatting specific to this implementation after the conversion of the DICOM file format to Nifti1 image format. This is done by a script written for this purpose. This specific portion of the pipeline requires manual work to accomplish. Once the script is run and the files converted to the proper format the data must then be uploaded to a server to then be downloaded.

The server of choice for this implementation is Amazon Web Service's Simple Secure Storage (S3). Once uploaded the files are then downloaded using the python client boto3.

METHOD

The first objective of the study is to test two key hypotheses. The first hypothesis is that NODDI is sensitive to AD related abnormality and hence NODDI values should be higher in controls than in patients with MCI (hypothesis 1). The second hypothesis is that if NODDI detects brain degeneration from AD, and MCI patients experience brain degeneration over the course of a year, ODI values should decrease from baseline to year later (the study of the ability to identify an individual with MI using longitudinal data), hypothesis 2. This hypothesis also

quantifies the magnitude of that change to identify a target for future therapies. What is not known is whether the degeneration is more rapid in patients than controls.

In order to produce data comparative to this situation we focused on patients who have been scanned at least two times with the appropriate types (T1 and DTI). This gives us a baseline and a year follow up to work with. With this data the null hypotheses can be tested. 73 patients were gathered in an even split between those diagnosed with control and MCI.

In summary, we proposed that the null hypothesis in hypothesis 1 is that there would be no difference between the control patients and the patients with MCI over the period of one year, whereas our alternative hypothesis indicates a statistically significant difference. The null hypothesis in hypothesis 2 is that there is not a detectable decline over a year. This could occur if timescale is long enough to detect a significant change. A secondary analysis may not be long enough to measure a significant change. A secondary analysis will examine whether the declines are greater in patients with MCI since they are undergoing a degenerative process.

The hypotheses are tested using the results from the NODDI algorithm referred to the Orientation Dispersion Index (ODI). ODI measures the dispersion of the axons and models, at that voxel, the orientation (be it varying from fanned to highly directional). The response variable consists of the a priori diagnosis of each patient group (i.e. control or MCI).

The second objective of our study is to build on the hypothesis that the use of the orientation dispersion index can produce group differences and as a result produce a predictor that can improve the sensitivity in discriminating patients with mild cognitive impairment from controls.

The results of each being set through a series of tests in order to produce incremental stages which would indicate the possibility of a statistically significant declaration.

The first of these steps being a statistical analysis using an ANCOVA test of the variables group (MCI, controls) and time (baseline, year 1). Due to the nature of brain degradation and the age differential indicated previously, the inclusion of age as a nuisance variable is a must in order to differentiate the group difference being purely age. An interaction of group and time variable tests whether the groups differ in change over time. Post hoc analyses should show that the difference between the time points should larger in patients with MCI than with controls.

Once our analysis indicates a statistically significant result, it will be evaluated using evaluated accuracy, receiver operating characteristic (ROC), and precision/recall values.

RESULTS

For our experiment the data gathered was ran through an Analysis of Covariance (ANCOVA) with a combination of time point (baseline, year 1) and diagnosis group (MCI, controls). A statistically significant t-test confirmed that individuals in the MCI group were older than individuals in the control group, age was included in the ANOVA as a nuisance variable/covariate.

Experiment One

We sought to analyze the differences between the two diagnosis groups. This group difference is seen to be the most sensitive. In this case, we sought to confirm this through using the ODI values resulting from the NODDI calculation. With group as the effect this resulted in a statistically significant indication as show in Table 2.

Repeated Measures Analysis of Variance with Effect Sizes and Powers

Effect	p	Observed power (alpha=0.05)
group	0.000325	0.961

Table 1: Observed Statistical Power of the Experiment 1

In the case of the statistical experiment 1 the null hypotheses can be soundly rejected with an observed power of 0.961 and a p-value < 0.05. As a result, it can be postulated that through NODDI analysis there exists a large difference between two groups. As the null hypotheses has been rejected verification can now commence.

The intent of the verification was to interrogate the group difference further. Using a regressor we intend to show the predictive power of this group difference. The prediction method we selected was a linear regression model. In order to indicate practicality, the use of the ODI value of each subject combined with the results other tests would prove that the combination could provide an increase in accuracy over use without.

The combination chosen was using the two tests previously described: RAVLT and MOCA. A sample size of 140 was produced and a linear regression model was trained with an equation shown in figure 8.

$$\text{regression} = 0.007 - 1.12\ \Delta ODI * \Delta MOCA * \Delta RAVLT + 0.0 * age_{57.4} - 0.005 * age_{58.7} + 1.82 * age_{61.2} + 0.981 * age_{61.5} + 0.031 * age_{62.3} + 0.993 * age_{62.9} + 1.013 * age_{65.0} - 0.118 * age_{65.5} + 0.127 * age_{66.0} + 0.548 * age_{66.8} + 0.993 * age_{67.3} - 0.004 * age_{67.4} - 0.056 * age_{67.9} - 0.007 * age_{68.2} - 0.005 * age_{69.0} + 0.993 * age_{69.1} - 0.007 * age_{69.3} + 0.035 * age_{69.5} + 0.993 * age_{69.6} - 0.057 * age_{69.8} - 0.006 * age_{70.2} + 0.056 * age_{70.3} + 0.028 * age_{70.6} - 0.007 * age_{70.7} + 0.862 * age_{71.1} + 0.469 * age_{71.2} - 0.007 * age_{71.4} + 0.980 * age_{71.6} + 0.837 * age_{71.7} + 0.993 * age_{71.9} - 0.49 * age_{72.2} + 0.984 * age_{72.3} - 0.010 * age_{72.6} + 0.187 * age_{73.6} - 0.007 * age_{74.0} + 1.007 * age_{74.5} - 0.008 * age_{75.3} + 0.023 * age_{75.7} - 0.007 * age_{76.3} + 1.089 * age_{76.4} + 1.003 * age_{76.7} + 0.973 * age_{76.8} + 0.995 * age_{77.3} - 0.034 * age_{77.4} + 0.945 * age_{78.2} + 0.993 * age_{78.5} + 0.993 * age_{79.5} + 0.992 * age_{79.8} + 1.151 * age_{79.9} + 0.993 * age_{80.3} - 0.007 * age_{80.6} - 0.019 * age_{81.2} + 0.998 * age_{81.4} + 1.019 * age_{81.9} + 0.003 * age_{82.7} + 1.013 * age_{82.9} + 0.993 * age_{84.1} + 0.995 * age_{85.3} - 0.007 * age_{86.3} + 0.972 * age_{86.8} + 0.969 * age_{88.6} + 1.68 * age_{89.1}$$

Figure 7: Regression Equation of Delta Values

The combined results produce an accuracy that beats current clinical evaluations with RAVLT by itself being 64% (Wood, Moodley, Lever, Minati, & Chan, 2016) and MOCA having a specificity of 70-73% (Dautzenberg, Lijmer, & Beekman, 2020; Masika, Yu, & Li, 2020).

This equation utilizes a delta for the ODI values, MOCA, and RAVLT over one year. Each age variable represents the individual ages of the patients pulled from ADNI. Results of this predictor for classification is detailed in table 4.

Accuracy	**ROC AUC**	**Average Precision**
83.08%	0.98	0.74

Table 2: Results of Regression Equation with Delta Values

The results of the model include an increased accuracy as well as an increased ROC AUC. The average precision has decreased 0.08. The ROC curve and the recall/precision curve have shifted even further to their desired positions.

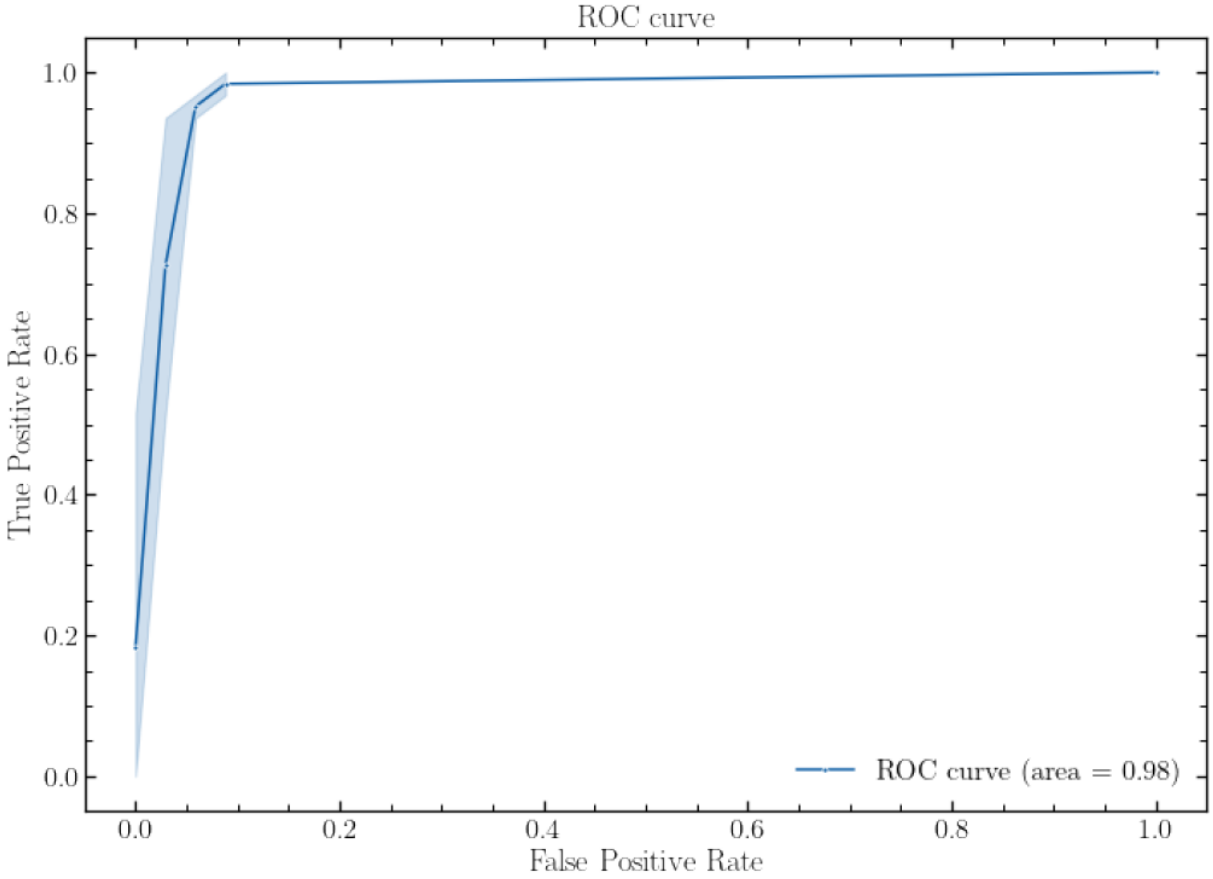

Figure 8: ROC curve for Regression Equation with Delta Values

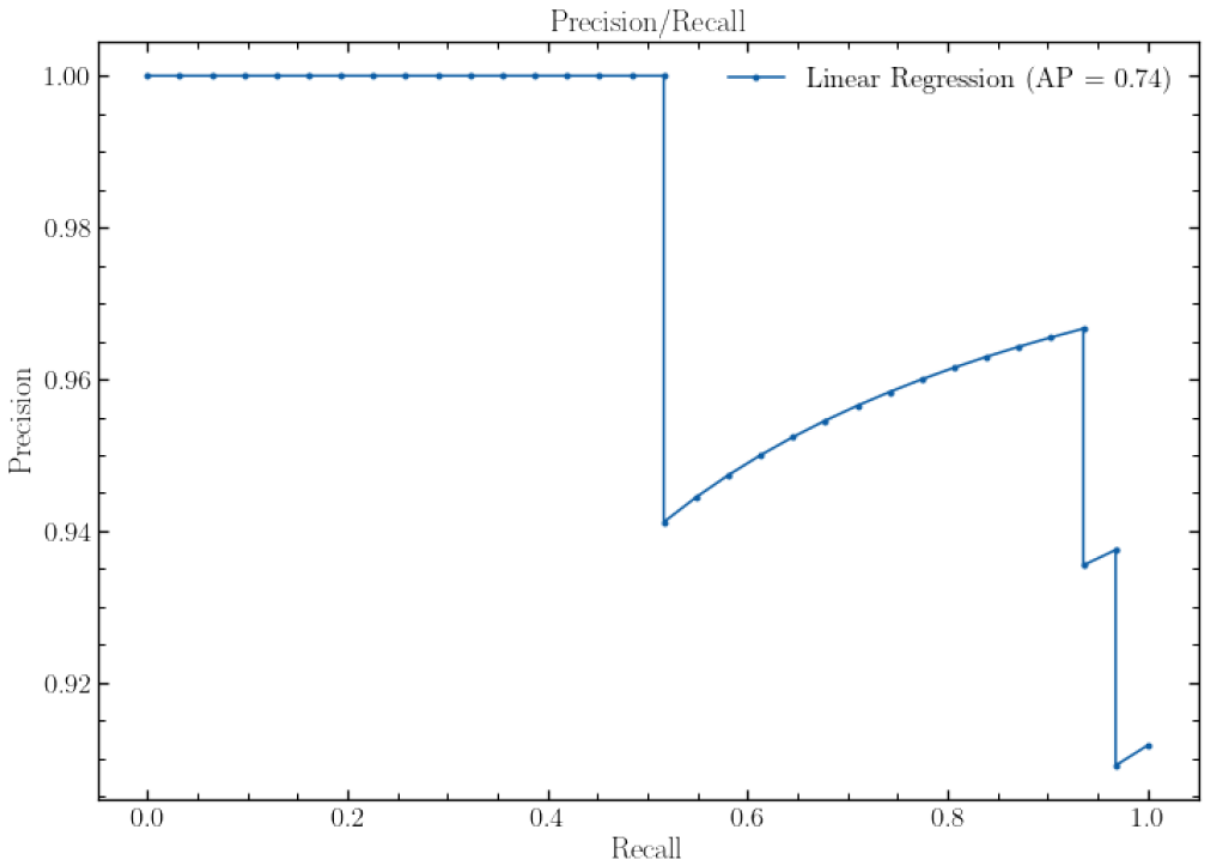

Figure 9: Recall/Precision for Regression Equation of Delta Values

In order to verify that this new equation's accuracy is contributed to the ODI values, testing without the ODI values included in the resulting equation resulted in the tests shown below:

$$\text{regression} = 0.030 - 0.00746\ \Delta RAVLT * \Delta MOCA + 0.0 * age_{57.4} - 0.045 * age_{58.7} + 0.523 * age_{61.2} + 0.993 * age_{61.5} - 0.104 * age_{62.3} + 0.970 * age_{62.9} + 0.881 * age_{65.0} - 0.097 * age_{65.5} + 0.179 * age_{66.0} + 0.470 * age_{66.8} + 0.970 * age_{67.3} - 0.082 * age_{67.4} + 0.134 * age_{67.9} - 0.030 * age_{68.2} + 0.019 * age_{69.0} + 0.970 * age_{69.1} - 0.015 * age_{69.3} + 0.067 * age_{69.5} + 0.970 * age_{69.6} - 0.328 * age_{69.8} + 0.067 * age_{70.2} + 0.194 * age_{70.3} - 0.060 * age_{70.6} - 0.030 * age_{70.7} + 1.104 * age_{71.1} + 0.683 * age_{71.2} - 0.030 * age_{71.4} + 0.963 * age_{71.6} + 0.791 * age_{71.7} + 1.015 * age_{71.9} - 0.664 * age_{72.2} + 0.911 * age_{72.3} - 0.052 * age_{72.6} - 0.093 * age_{73.6} - 0.030 * age_{74.0} + 1.060 * age_{74.5} - 0.037 * age_{75.3} + 0.000 * age_{75.7} - 0.030 * age_{76.3} + 1.910 * age_{76.4} + 0.985 * age_{76.7} + 0.332 * age_{76.8} + 0.940 * age_{77.3} + 0.060 * age_{77.4} + 1.030 * age_{78.2} + 0.970 * age_{78.5} + 0.970 * age_{79.5} + 0.918 * age_{79.8} + 1.820 * age_{79.9} + 0.970 * age_{80.3} - 0.030 * age_{80.6} + 0.060 * age_{81.2} + 0.978 * age_{81.4} + 1.060 * age_{81.9} - 0.119 * age_{82.7} + 1.082 * age_{82.9} + 0.970 * age_{84.1} + 0.851 * age_{85.3} - 0.030 * age_{86.3} + 0.925 * age_{86.8} + 0.702 * age_{88.6} + 0.120 * age_{89.1}$$

Figure 10: Verification Regression Equation without Delta ODI Values

In this new equation the Delta ODI values was removed, and a new linear regression model was trained. The overview of the performance of this model is shown in table 5.

Accuracy	**ROC AUC**	**Average Precision**
78.46%	1.0	0.69

Table 3: Classification of results on model excluding Delta ODI

The accuracy has reduced 4.62 percent. The area under the curve has increase 0.02 and the average precision has decreased 0.05. This result shows a contribution via the inclusion of the ODI values.

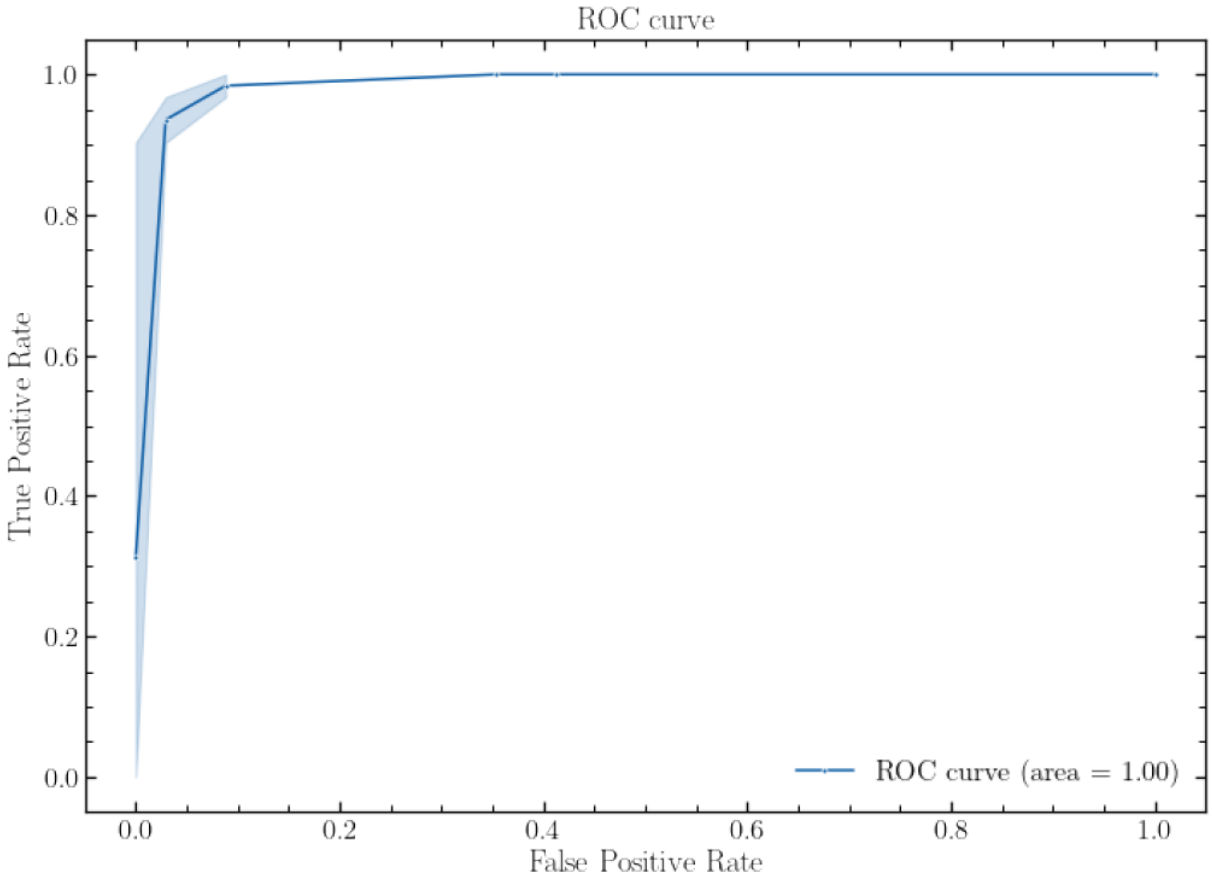

Figure 11: ROC Curve for Regression without Delta ODI Values

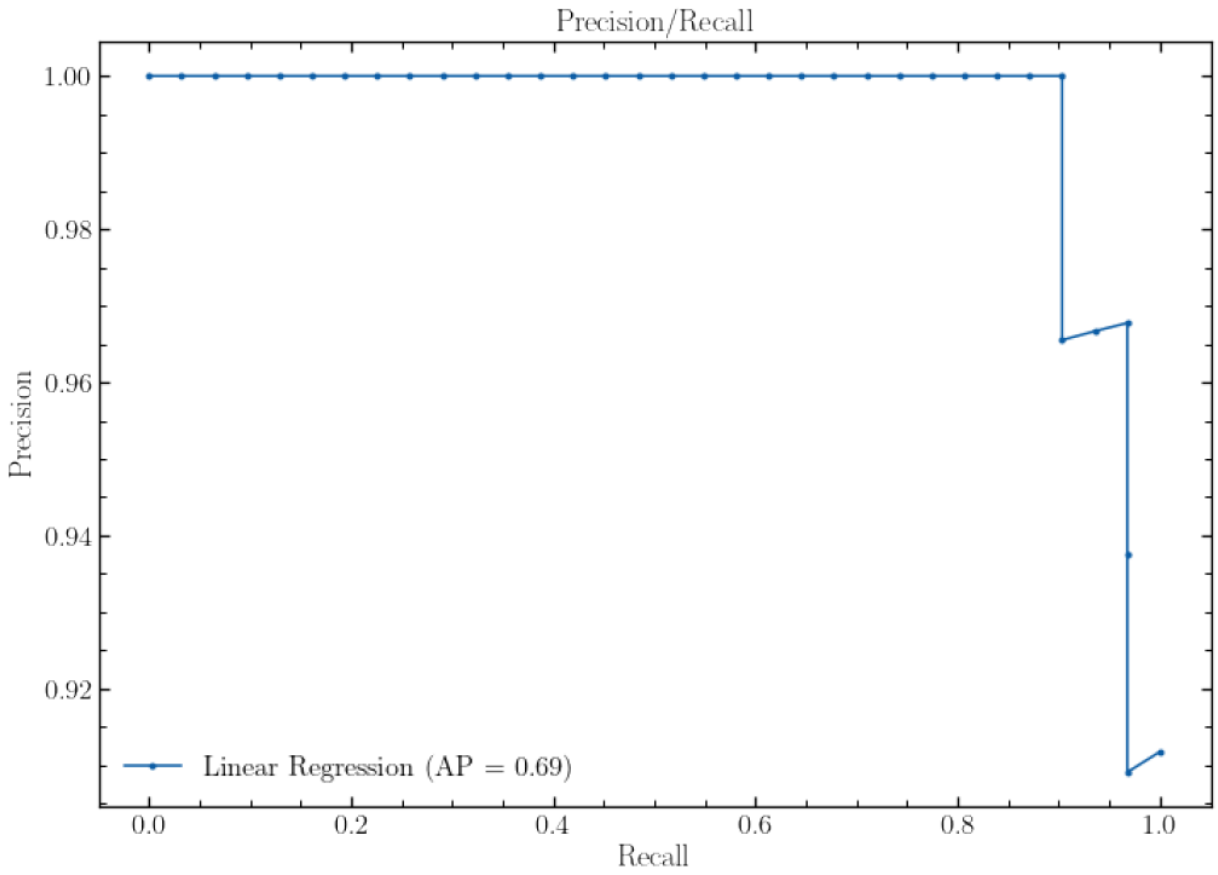

Figure 12: Precision/Recall of Regression Equation without ODI Values

Hypothesis 2: Degeneration

In the second experiment we sought to confirm a change over time in each diagnosis group. Through the use of an ANCOVA we analyzed the effect of both time and group and found that the degeneration experienced by the MCI group was not of a statistically significant difference of the control group. This resulted in a small power (p-value > 0.05), as shown in Table 4.

Repeated Measures Analysis of Variance with Effect Sizes and Powers

Effect	P	Observed power (alpha=0.05)
*TIME*group*	0.306	0.174

Table 4: Power of Group Differences Over Time

Our alternative hypothesis states that there was a statically change over time. We observed no such change in this cohort.

DISCUSSION

The most robust finding of our study is that ODI values were lower in patients with MCI than those in the control group, confirming hypothesis 1, which states that this value is sensitive to abnormality in the medial temporal lobe. A linear regression equation further interrogated whether using ODI as a metric improves the diagnosis accuracy. The diagnostic ability of the trained classifier was evaluated using a ROC curve, accuracy, and average precision. Neither ODI change over one year or group differences between ODI changes were statistically significant.

The findings of the study which confirmed hypothesis 1 was validated using linear regression. Two models were trained on the dataset generated: one trained with the inclusion of the ODI values and one without. Through the inclusion of the ODI values, the model showed a marked improvement in accuracy as compared to the model trained without.

CONCLUSION

Our study demonstrates that NODDI is an excellent method of differentiating between the diseased and healthy individuals. Its ability to further characterize the

different tissues of the patients allows for a more in-depth and robust analysis of the patient cohort.

FUTURE WORK

Whereas longitudinal change in ODI was too small to detect a future reanalysis of data over two or three years may reveal a change. An examination of the raw difference scores suggested that the patients with MCI may have experience so much decline that their year 1 may reflect a floor effect in which those scores may not have farther to fall and the sensitivity of this NODDI analysis may be earlier in the disease state. For example, the analysis may be useful in identifying which of the healthy controls will later progress.

ACKNOWLEDGEMENTS

In accordance with the ADNI Data Use Agreement the following acknowledgements are made. Data collection and sharing for this project was funded by the Alzheimer's Disease Neuroimaging Initiative (ADNI) (National Institutes of Health Grant U01 AG024904) and DOD ADNI (Department of Defense award number W81XWH-12-2-0012). ADNI is funded by the National Institute on Aging, the National Institute of Biomedical Imaging and Bioengineering, and through generous contributions from the following: AbbVie, Alzheimer’s Association; Alzheimer’s Drug Discovery Foundation; Araclon Biotech; BioClinica, Inc.; Biogen; Bristol-Myers Squibb Company; CereSpir, Inc.; Cogstate; Eisai Inc.; Elan Pharmaceuticals, Inc.; Eli Lilly and Company; EuroImmun; F. Hoffmann-La Roche Ltd and its affiliated company Genentech, Inc.; Fujirebio; GE Healthcare; IXICO Ltd.; Janssen Alzheimer Immunotherapy

Research & Development, LLC.; Johnson & Johnson Pharmaceutical Research & Development LLC.; Lumosity; Lundbeck; Merck & Co., Inc.; Meso Scale Diagnostics, LLC.; NeuroRx Research; Neurotrack Technologies; Novartis Pharmaceuticals Corporation; Pfizer Inc.; Piramal Imaging; Servier; Takeda Pharmaceutical Company; and Transition Therapeutics. The Canadian Institutes of Health Research is providing funds to support ADNI clinical sites in Canada. Private sector contributions are facilitated by the Foundation for the National Institutes of Health (www.fnih.org). The grantee organization is the Northern California Institute for Research and Education, and the study is coordinated by the Alzheimer's Therapeutic Research Institute at the University of Southern California. ADNI data are disseminated by the Laboratory for Neuro Imaging at the University of Southern California.

REFERENCE

Albert, M. S., DeKosky, S. T., Dickson, D., Dubois, B., Feldman, H. H., Fox, N. C., . . . Phelps, C. H. (2011). The diagnosis of mild cognitive impairment due to Alzheimer's disease: recommendations from the National Institute on Aging-Alzheimer's Association workgroups on diagnostic guidelines for Alzheimer's disease. *Alzheimers Dement, 7*(3), 270-279. doi:10.1016/j.jalz.2011.03.008

Andersson, J. L. R., & Sotiropoulos, S. N. (2016). An integrated approach to correction for off-resonance effects and subject movement in diffusion MR imaging. *Neuroimage, 125*, 1063-1078. doi:10.1016/j.neuroimage.2015.10.019

Assaf, Y., & Basser, P. J. (2005). Composite hindered and restricted model of diffusion (CHARMED) MR imaging of the human brain. *Neuroimage, 27*(1), 48-58. doi:10.1016/j.neuroimage.2005.03.042

Assaf, Y., & Cohen, Y. (2000). Assignment of the water slow-diffusing component in the central nervous system using q-space diffusion MRS: implications for fiber tract imaging. *Magn Reson Med, 43*(2), 191-199. doi:10.1002/(sici)1522-2594(200002)43:2<191::aid-mrm5>3.0.co;2-b

Assaf, Y., Freidlin, R. Z., Rohde, G. K., & Basser, P. J. (2004). New modeling and experimental framework to characterize hindered and restricted water diffusion in brain white matter. *Magn Reson Med, 52*(5), 965-978. doi:10.1002/mrm.20274

Barazany, D., Basser, P. J., & Assaf, Y. (2009). In vivo measurement of axon diameter distribution in the corpus callosum of rat brain. *Brain, 132*(Pt 5), 1210-1220. doi:10.1093/brain/awp042

Basser, P. J., Mattiello, J., & LeBihan, D. (1994a). Estimation of the effective self-diffusion tensor from the NMR spin echo. *J Magn Reson B, 103*(3), 247-254. doi:10.1006/jmrb.1994.1037

Basser, P. J., Mattiello, J., & LeBihan, D. (1994b). MR diffusion tensor spectroscopy and imaging. *Biophys J, 66*(1), 259-267. doi:10.1016/S0006-3495(94)80775-1

Bateman, R. J., Xiong, C., Benzinger, T. L., Fagan, A. M., Goate, A., Fox, N. C., . . . Dominantly Inherited Alzheimer, N. (2012). Clinical and biomarker changes in dominantly inherited Alzheimer's disease. *N Engl J Med, 367*(9), 795-804. doi:10.1056/NEJMoa1202753

Behrens, T. E., Woolrich, M. W., Jenkinson, M., Johansen-Berg, H., Nunes, R. G., Clare, S., . . . Smith, S. M. (2003). Characterization and propagation of uncertainty in diffusion-weighted MR imaging. *Magn Reson Med, 50*(5), 1077-1088. doi:10.1002/mrm.10609

Bischkopf, J., Busse, A., & Angermeyer, M. C. (2002). Mild cognitive impairment--a review of prevalence, incidence and outcome according to current approaches. *Acta Psychiatr Scand, 106*(6), 403-414. doi:10.1034/j.1600-0447.2002.01417.x

Bozzali, M., Falini, A., Franceschi, M., Cercignani, M., Zuffi, M., Scotti, G., . . . Filippi, M. (2002). White matter damage in Alzheimer's disease assessed in vivo using diffusion tensor magnetic resonance imaging. *J Neurol Neurosurg Psychiatry, 72*(6), 742-746. doi:10.1136/jnnp.72.6.742

Brett, M., Johnsrude, I. S., & Owen, A. M. (2002). The problem of functional localization in the human brain. *Nat Rev Neurosci, 3*(3), 243-249. doi:10.1038/nrn756

Brookmeyer, R., Johnson, E., Ziegler-Graham, K., & Arrighi, H. M. (2007). Forecasting the global burden of Alzheimer's disease. *Alzheimers Dement, 3*(3), 186-191. doi:10.1016/j.jalz.2007.04.381

Dautzenberg, G., Lijmer, J., & Beekman, A. (2020). Diagnostic accuracy of the Montreal Cognitive Assessment (MoCA) for cognitive screening in old age psychiatry: Determining cutoff scores in clinical practice. Avoiding spectrum bias caused by healthy controls. *Int J Geriatr Psychiatry, 35*(3), 261-269. doi:10.1002/gps.5227

Estevez-Gonzalez, A., Kulisevsky, J., Boltes, A., Otermin, P., & Garcia-Sanchez, C. (2003). Rey verbal learning test is a useful tool for differential diagnosis in the preclinical phase of Alzheimer's disease: comparison with mild cognitive impairment and normal aging. *Int J Geriatr Psychiatry, 18*(11), 1021-1028. doi:10.1002/gps.1010

FAQ | MoCA Montreal - Cognitive Assessment. (2020). Retrieved from https://www.mocatest.org/faq/

Fick, R. H. J., Wassermann, D., & Deriche, R. (2019). The Dmipy Toolbox: Diffusion MRI Multi-Compartment Modeling and Microstructure Recovery Made Easy. *Front Neuroinform, 13*, 64. doi:10.3389/fninf.2019.00064

Garyfallidis, E., Brett, M., Amirbekian, B., Rokem, A., van der Walt, S., Descoteaux, M., . . . Dipy, C. (2014). Dipy, a library for the analysis of diffusion MRI data. *Front Neuroinform, 8*, 8. doi:10.3389/fninf.2014.00008

Goldman, J. G., Bledsoe, I. O., Merkitch, D., Dinh, V., Bernard, B., & Stebbins, G. T. (2017). Corpus callosal atrophy and associations with cognitive impairment in Parkinson disease. *Neurology, 88*(13), 1265-1272. doi:10.1212/WNL.0000000000003764

Golomb, J., Kluger, A., & Ferris, S. H. (2004). Mild cognitive impairment: historical development and summary of research. *Dialogues Clin Neurosci, 6*(4), 351-367. Retrieved from https://www.ncbi.nlm.nih.gov/pubmed/22034453

Hua, K., Zhang, J., Wakana, S., Jiang, H., Li, X., Reich, D. S., . . . Mori, S. (2008). Tract probability maps in stereotaxic spaces: analyses of white matter anatomy and tract-specific quantification. *Neuroimage, 39*(1), 336-347. doi:10.1016/j.neuroimage.2007.07.053

Jalbert, J. J., Daiello, L. A., & Lapane, K. L. (2008). Dementia of the Alzheimer type. *Epidemiol Rev, 30*, 15-34. doi:10.1093/epirev/mxn008

Jenkinson, M., Bannister, P., Brady, M., & Smith, S. (2002). Improved optimization for the robust and accurate linear registration and motion correction of brain images. *Neuroimage, 17*(2), 825-841. doi:10.1016/s1053-8119(02)91132-8

Jenkinson, M., & Smith, S. (2001). A global optimisation method for robust affine registration of brain images. *Med Image Anal, 5*(2), 143-156. doi:10.1016/s1361-8415(01)00036-6

Knopman, D. S., & Petersen, R. C. (2014). Mild cognitive impairment and mild dementia: a clinical perspective. *Mayo Clin Proc, 89*(10), 1452-1459. doi:10.1016/j.mayocp.2014.06.019

Lyketsos, C. G., Colenda, C. C., Beck, C., Blank, K., Doraiswamy, M. P., Kalunian, D. A., . . . Task Force of American Association for Geriatric, P. (2006). Position statement of the American Association for Geriatric

Psychiatry regarding principles of care for patients with dementia resulting from Alzheimer disease. *Am J Geriatr Psychiatry, 14*(7), 561-572. doi:10.1097/01.JGP.0000221334.65330.55
Masika, G. M., Yu, D. S. F., & Li, P. W. C. (2020). Accuracy of the Montreal Cognitive Assessment in Detecting Mild Cognitive Impairment and Dementia in the Rural African Population. *Arch Clin Neuropsychol*. doi:10.1093/arclin/acz086
Michael M. McKerns, L. S., Tim Sullivan, Alta Fang, Michael A.G. Aivazis. (2012). Building a Framework for Predictive Science.
Michael McKerns, M. A. (2010-). pathos: a framework for heterogeneous computing.
Miller, M. I., Ratnanather, J. T., Tward, D. J., Brown, T., Lee, D. S., Ketcha, M., . . . Team, B. R. (2015). Network Neurodegeneration in Alzheimer's Disease via MRI Based Shape Diffeomorphometry and High-Field Atlasing. *Front Bioeng Biotechnol, 3*, 54. doi:10.3389/fbioe.2015.00054
Moradi, E., Hallikainen, I., Hanninen, T., Tohka, J., & Alzheimer's Disease Neuroimaging, I. (2017). Rey's Auditory Verbal Learning Test scores can be predicted from whole brain MRI in Alzheimer's disease. *Neuroimage Clin, 13*, 415-427. doi:10.1016/j.nicl.2016.12.011
Nagae-Poetscher, S. M. S. W. P. C. M. v. Z. L. M. (2005). *MRI Atlas of Human White Matter*.
Nasreddine, Z. S., Phillips, N. A., Bedirian, V., Charbonneau, S., Whitehead, V., Collin, I., . . . Chertkow, H. (2005). The Montreal Cognitive Assessment, MoCA: a brief screening tool for mild cognitive impairment. *J Am Geriatr Soc, 53*(4), 695-699. doi:10.1111/j.1532-5415.2005.53221.x
Neugroschl, J., & Wang, S. (2011). Alzheimer's disease: diagnosis and treatment across the spectrum of disease severity. *Mt Sinai J Med, 78*(4), 596-612. doi:10.1002/msj.20279
Panagiotaki, E., Schneider, T., Siow, B., Hall, M. G., Lythgoe, M. F., & Alexander, D. C. (2012). Compartment models of the diffusion MR signal in brain white matter: a taxonomy and comparison. *Neuroimage, 59*(3), 2241-2254. doi:10.1016/j.neuroimage.2011.09.081
Petersen, R. C., Doody, R., Kurz, A., Mohs, R. C., Morris, J. C., Rabins, P. V., . . . Winblad, B. (2001). Current concepts in mild cognitive impairment. *Arch Neurol, 58*(12), 1985-1992. doi:10.1001/archneur.58.12.1985
Petersen, R. C., Smith, G. E., Waring, S. C., Ivnik, R. J., Tangalos, E. G., & Kokmen, E. (1999). Mild cognitive impairment: clinical characterization and outcome. *Arch Neurol, 56*(3), 303-308. doi:10.1001/archneur.56.3.303
Petersen, R. C., Stevens, J. C., Ganguli, M., Tangalos, E. G., Cummings, J. L., & DeKosky, S. T. (2001). Practice parameter: early detection of dementia:

mild cognitive impairment (an evidence-based review). Report of the Quality Standards Subcommittee of the American Academy of Neurology. *Neurology, 56*(9), 1133-1142. doi:10.1212/wnl.56.9.1133

Pfeffer, R. I., Kurosaki, T. T., Harrah, C. H., Jr., Chance, J. M., & Filos, S. (1982). Measurement of functional activities in older adults in the community. *J Gerontol, 37*(3), 323-329. doi:10.1093/geronj/37.3.323

Rabin, L. A., Pare, N., Saykin, A. J., Brown, M. J., Wishart, H. A., Flashman, L. A., & Santulli, R. B. (2009). Differential memory test sensitivity for diagnosing amnestic mild cognitive impairment and predicting conversion to Alzheimer's disease. *Neuropsychol Dev Cogn B Aging Neuropsychol Cogn, 16*(3), 357-376. doi:10.1080/13825580902825220

Rivas-Vazquez, R. A., Mendez, C., Rey, G. J., & Carrazana, E. J. (2004). Mild cognitive impairment: new neuropsychological and pharmacological target. *Arch Clin Neuropsychol, 19*(1), 11-27. Retrieved from https://www.ncbi.nlm.nih.gov/pubmed/14670376

Roberts, R. O., Knopman, D. S., Mielke, M. M., Cha, R. H., Pankratz, V. S., Christianson, T. J., . . . Petersen, R. C. (2014). Higher risk of progression to dementia in mild cognitive impairment cases who revert to normal. *Neurology, 82*(4), 317-325. doi:10.1212/WNL.0000000000000055

Schmidt, M. (1996). Rey auditory verbal learning test: A handbook. *Los Angeles, CA: Western Psychological Services.*

Selnes, P., Aarsland, D., Bjornerud, A., Gjerstad, L., Wallin, A., Hessen, E., . . . Fladby, T. (2013). Diffusion tensor imaging surpasses cerebrospinal fluid as predictor of cognitive decline and medial temporal lobe atrophy in subjective cognitive impairment and mild cognitive impairment. *J Alzheimers Dis, 33*(3), 723-736. doi:10.3233/JAD-2012-121603

Soares, J. M., Marques, P., Alves, V., & Sousa, N. (2013). A hitchhiker's guide to diffusion tensor imaging. *Front Neurosci, 7*, 31. doi:10.3389/fnins.2013.00031

Teng, E., Becker, B. W., Woo, E., Knopman, D. S., Cummings, J. L., & Lu, P. H. (2010). Utility of the functional activities questionnaire for distinguishing mild cognitive impairment from very mild Alzheimer disease. *Alzheimer Dis Assoc Disord, 24*(4), 348-353. doi:10.1097/WAD.0b013e3181e2fc84

Tournier, J. D., Mori, S., & Leemans, A. (2011). Diffusion tensor imaging and beyond. *Magn Reson Med, 65*(6), 1532-1556. doi:10.1002/mrm.22924

van Duijn, C. M. (1996). Epidemiology of the dementias: recent developments and new approaches. *J Neurol Neurosurg Psychiatry, 60*(5), 478-488. doi:10.1136/jnnp.60.5.478

Wakana, S., Caprihan, A., Panzenboeck, M. M., Fallon, J. H., Perry, M., Gollub, R. L., . . . Mori, S. (2007). Reproducibility of quantitative tractography

methods applied to cerebral white matter. *Neuroimage, 36*(3), 630-644. doi:10.1016/j.neuroimage.2007.02.049
Wen, Q., Mustafi, S. M., Li, J., Risacher, S. L., Tallman, E., Brown, S. A., . . . Wu, Y. C. (2019). White matter alterations in early-stage Alzheimer's disease: A tract-specific study. *Alzheimers Dement (Amst), 11*, 576-587. doi:10.1016/j.dadm.2019.06.003
Wood, R. A., Moodley, K. K., Lever, C., Minati, L., & Chan, D. (2016). Allocentric Spatial Memory Testing Predicts Conversion from Mild Cognitive Impairment to Dementia: An Initial Proof-of-Concept Study. *Front Neurol, 7*, 215. doi:10.3389/fneur.2016.00215
Zhang, H., Schneider, T., Wheeler-Kingshott, C. A., & Alexander, D. C. (2012). NODDI: practical in vivo neurite orientation dispersion and density imaging of the human brain. *Neuroimage, 61*(4), 1000-1016. doi:10.1016/j.neuroimage.2012.03.072

APPENDICES

APPENDIX A

RAVLT

During the RAVLT the examiner reads a list of words and after hearing the list of words, the patient needs to repeat those words back. After several trials of this immediate recall, there is a 20-minute delay and then the patient is asked to recall the items on the list they previously rehearsed.

RAVLT is broken into two sections: Immediate and Percent Forgetting. A patient's Immediate recall score is the sum of all the items correctly recalled on all the five immediate recall trials. The delayed recall is the number of items recalled after this delay. An assumption is that with brain atrophy associated with degeneration smaller brain regions are associated with worse functioning. This key finding is due to the role the medial temporal lobe plays in memory and shows the power of RAVLT to indicate a decline in the memory portion of the brain thus providing a powerful predictor in early Alzheimer's.

APPENDIX B

MoCA

For reference, a patient classified as one with normal cognition will have a score of 26 or over. A cut-off score of 18 is considered to this threshold between patients with MCI from AD, whereas the average score for MCI is 22 with a range between 19-25 and 16 for mild AD with a range of 11-21 ("FAQ | MoCA Montreal - Cognitive Assessment," 2020). When a more intact level on this range is recorded it acts as confirmation that the patient is still at the stage of MCI.

APPENDIX C

Grey and White Matter

Grey matter is comprised of neuron bodies and white matter is comprised of the connections between neurons or axons. These white matter brain regions appear to be white because the axonal fiber tracts are supported and insulated by glia that surround the axons. Much like an electric wire conducts more effectively because it is surrounded by insulation, neurons function more effectively when the axons that need to conduct brain signals (action potentials) are insulated by glia.

A white matter fiber tract is a group of axons. The groups travel between different brain regions which suggests that there is communication between these brain regions. This provides an important clue about how the regions function and how brain pathology disrupts this process.

APPENDIX D

Diffusion Tensor Imaging

Diffusion Tensor Imaging processing includes a series of steps of which completes with a tensor estimation phase. This phase uses estimation procedures like Ordinary Least Squares in order to produce the voxel's eigenvalues and eigenvectors. A voxel's diffusion tensor represents the base direction and magnitude of the voxel at each point in the brain. These directions and magnitudes are generated from a 3x3 symmetric matrix.

Once the tensor is estimated and the brain is modeled, different diffusion characteristics are modeled. Of the three tissue types, white matter in the brain is characterized by less diffusion restriction but tends to be directionally dependent whereas grey matter tends be less directionally dependent. Lastly Cerebral Spinal Fluid tends to freely diffuse is every direction.

These different inherent characteristics of the three tissue types make possible modeling tracts and the directions of these voxels over a distance and leading to analysis such as tractography that maps entire bundles of axons throughout the brain and can give an accurate representation of the internal structure and architecture of connections between brain regions.

Included with the tractography analysis are a variety of summary statistics resulting from Diffusion Tensor Imaging. These statistics include two main statistics: Mean Diffusivity (MD) and Fractional Anisotropy (FA). Analysis of these statistics are usually done in a region of interest manor specifying the area of the brain to study. Of these areas, higher MD models an increase of diffusion whereas lower FA indicates and lack of cohesion in that region (Soares et al., 2013).

APPENDIX E

Diffusion Compartmental Imaging

Diffusion Compartment Imaging is a relatively new subset of techniques to analyze Diffusion Weighted Images. DCI's purpose is to utilize a complex combination of different models, each whose purpose is analyzing voxels of different tissue types found in the brain of which are divided up into intra-cellular space, extra-cellular space (Zhang et al., 2012).

Extra-cellular space is mostly defined as the cellular membranes of somas and glial cells, whereas Intra-cellular space is defined as space bounded by axonal and dendritic membranes (Zhang et al., 2012). Each of these cellular types harkens back to the two distinctions (free diffusion and restricted diffusion) of the tissues in the brain and identifies the different types of restrictions present: Hindered and Restricted. Hindered diffusion points to the pattern found in the extra-cellular space whereas Restricted diffusion points to the intra-cellular space (Assaf & Cohen, 2000).

The distinction between these two spaces found in Diffusion Weighted Images and the types therein produces a model of the brain that is more complex than a generalized model of the three types of tissues. In-order to properly analyze this distinction a model must include these characteristics, but in what way should these distinctions be modeled?

The Diffusion Tensor Imaging method of modeling is to build a symmetrical tensor for each voxel. This symmetrical tensor is modeled with three three-dimensional vectors representing the directions of flow usually in a single distinct direction. This highly specific direction does not consider a possible distribution of values over these axes.

Several implementations have been proposed to provide this distinction to better model different types of diffusion in the brain using various shapes. These shapes

have their own distributions and characteristics akin to different intra- and extra-cellular components.

One such model is the ball and stick model (Behrens et al., 2003). The distinction between the intra-cellular and extra-cellular compartments are made using a stick and ball representation. The stick, being a cylinder of zero radius, is used to model the highly restrictive intra-cellular components, whereas the ball is utilized to model the hindered extra-cellular component (Behrens et al., 2003; Panagiotaki et al., 2012). Based on the knowledge of the intra-cellular region being highly restricted and directional, the stick model portrays this distinction representing each voxel to lie on a path that is geometrically restricted. The ball in this case portrays the highly diffuse nature of the extra-cellular compartment as the direction of diffusion is less strict in these regions.

Another model named CHARMED or Composite Hindered And Restricted Model of Diffusion (CHARMED) utilizes an impermeable ideal cylinder whose radius matches a gamma distribution (Assaf & Basser, 2005; Assaf, Freidlin, Rohde, & Basser, 2004; Panagiotaki et al., 2012; Zhang et al., 2012). This idealized cylinder represents the intra-cellular compartment. The extra-cellular compartment is represented by a non-directionally dependent value.

A simplified version of CHARMED was proposed by Alexander (2008) which reduces the complexity of the gamma distribution to a single radius. This keeps the form of the cylinder for the intra-cellular representation and a shape of a Zeppelin for use in the extra-cellular area. The introduction of the Zeppelin keeps the directionally independent nature of the extra-cellular area but introduces a symmetric component about an axis. Later additions were made to the CHARMED model in the addition of another compartment: free-water. The intent of this

compartment was to obtain the minimal model of white matter diffusion coined as MMWMD (Barazany, Basser, & Assaf, 2009).

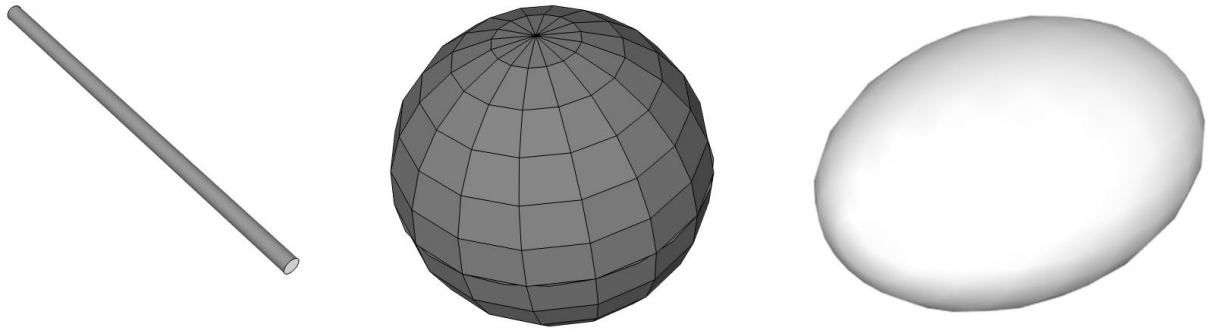

Figure 13: The Stick, Ball, and Zeppelin model

With each implementation the concept of a distinct shape representing the distinct restrictions is paramount. The Ball & Stick method, plus the simplification of the CHARMED model with a Zeppelin for the extra-cellular component represents the crux of the next model proposed. NODDI or Neurite Orientation Density Dispersion Index provides a combination of these models (Zhang et al., 2012).

In the case of the Intra-cellular model the highly restrictive nature is modeled using a Watson distributed distribution of sticks. This allowed for the modeling in instances where axons are either highly parallel to other bundles like in the corpus callosum to instances where the intra-cellular component consists of fans and bends as in the centrum semiovale (Zhang et al., 2012).

For the extra-cellular model, the compartment is modeled using an orientation-dispersed cylinder or Zeppelin. The Zeppelin is also modeled using a Watson distribution. Lastly, in keeping with the three types of tissues in the brain, the CSF or Cerebral Spinal Fluid is modeled using a Ball to represent the lack of directional dependence on the count of the diffusion for that region.

The result of the NODDI calculation, much like DTI, produces a summary statistic: Orientation Dispersion Index (ODI). The ODI value consists of a range

between 0 and 1 bounded by a Watson distribution which measures the dispersion of each voxel's orientation. A higher ODI value indicates lower diffusion at the point of the voxel of which indicate an intact white matter tract. A decrease found in ODI would indicate water diffusing more freely due to not being constrained by intact white matter tracts and as a result should reflect degeneration.

Comparisons

The comparisons between the summary statistic generated by DTI and the ODI generated by NODDI was the topic of a recent study by (Wen et al., 2019). This study focused on a numerous amount of tract data produced through a cohort of patients with no complications to patients with mild cognitive impairment. The key contribution taken away from this study was the vast number of tracts studied in their analysis. The study contained an analysis of 27 tracks of patients with early-stage Alzheimer's disease. Of these tracks Wen et al. (2019) found that the tracks with the highest predictive power to discriminate groups were found in the parahippocampal cingulum, thalamic radiation, and forceps major region of the brain.

An addition comparison between DTI, NODDI, and q-space analysis resulted with DTI being the most sensitive in its ability to produce a characterization of the degradation but found that NODDI and q-space still characterized the degradation.

With the a-priori analysis produced by Wen et al. (2019) we proceed with an analysis of a variety of patients of which include an even distribution of control and those diagnosed with MCI the goal of which is to utilize RAVLT and MOCA as well as NODDI to produce a group difference between the two that is invariant to possible attributes like age.